INSTITUTE OF PHYSICS PUBLISHING PHYSIOLOGICAL MEASUREMENT

Physiol. Meas. **26** (2005) 875–884 doi:10.1088/0967-3334/26/5/023

Noise analysis in magnetic resonance electrical impedance tomography at 3 and 11 T field strengths

Rosalind Sadleir[1], Samuel Grant[2], Sung Uk Zhang[1], Byung Il Lee[3], Hyun Chan Pyo[3], Suk Hoon Oh[3], Chunjae Park[3], Eung Je Woo[3,4], Soo Yeol Lee[3], Ohin Kwon[4] and Jin Keun Seo[5]

[1] Department of Biomedical Engineering, University of Florida, Gainesville, FL, USA
[2] Department of Neuroscience, University of Florida, Gainesville, FL, USA
[3] College of Electronics and Information, Kyung Hee University, Seoul, Korea
[4] Department of Mathematics, Konkuk University, Seoul, Korea
[5] Department of Mathematics, Yonsei University, Seoul, Korea

E-mail: ejwoo@khu.ac.kr

Received 7 May 2005, accepted for publication 19 July 2005
Published 8 August 2005
Online at stacks.iop.org/PM/26/875

Abstract

In magnetic resonance electrical impedance tomography (MREIT), we measure the induced magnetic flux density inside an object subject to an externally injected current. This magnetic flux density is contaminated with noise, which ultimately limits the quality of reconstructed conductivity and current density images. By analysing and experimentally verifying the amount of noise in images gathered from two MREIT systems, we found that a carefully designed MREIT study will be able to reduce noise levels below 0.25 and 0.05 nT at main magnetic field strengths of 3 and 11 T, respectively, at a voxel size of $3 \times 3 \times 3$ mm^3. Further noise level reductions can be achieved by optimizing MREIT pulse sequences and using signal averaging. We suggest two different methods to estimate magnetic flux noise levels, and the results are compared to validate the experimental setup of an MREIT system.

Keywords: electrical impedance tomography, magnetic flux density, MRI, MREIT, noise analysis

1. Introduction

When current is injected into an electrically conducting object, it generates voltage, current density and magnetic flux density distributions. These distributions are determined by the geometry, electrode configuration and conductivity distribution of the object. Based on these fundamental electromagnetic principles, magnetic resonance electrical impedance tomography (MREIT) is being developed as a method of generating cross-sectional images of conductivity

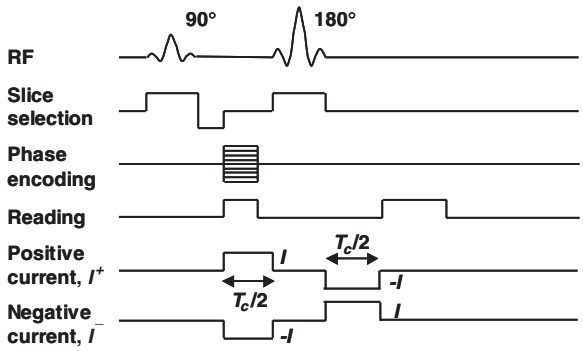

Figure 1. Spin echo pulse sequence for MREIT.

and current density distributions (Zhang 1992, Woo *et al* 1994, Ider and Birgul 1998, Ider *et al* 2003, Kwon *et al* 2002, Khang *et al* 2002, Lee *et al* 2003a). The basic data is the internal magnetic flux density data measured by an MRI scanner. Several MREIT image reconstruction algorithms have been developed based on measurements of only one component of the induced internal magnetic flux density $\mathbf{B} = (B_x, B_y, B_z)$ subject to multiple injection currents (Seo *et al* 2003, Ider and Onart 2004, Oh *et al* 2003, Park *et al* 2004a, 2004b, Kwon *et al* 2005).

Recent experimental studies in MREIT have demonstrated that conductivity and current density imaging with a spatial resolution comparable to that of MR images is possible as long as we inject enough current into the imaging object in order to induce B_z signals with enough signal-to-noise ratio (SNR) (Oh *et al* 2003, 2004, 2005). Safety requirements (Reilly 1998) suggest that we need to reduce injection current magnitude to make the technique clinically applicable. This implies that we must develop experimental and data processing techniques to minimize noise in B_z data.

With the goal of minimizing the noise level, and thereby the amount of injection current, this paper presents a new noise analysis for MREIT. Both theoretical and experimental methods of estimating the noise level in measured B_z data are derived and MREIT experiments were performed at both 3 and 11 T field strengths to verify these derivations. Based on the results, we discuss different ways to reduce noise levels in MREIT.

The noise analysis described in this paper will be followed with an investigation of the effects of noise on image quality. Some form of sensitivity analysis must be derived to determine the smallest local change in conductivity that can be accurately imaged. These analyses must take into consideration relationships between the induced magnetic flux density, size and shape of the imaging object, amount of injected current, electrode configuration, image reconstruction algorithm, amongst other factors.

2. Methods

2.1. Noise estimation method 1

The spin echo pulse sequence shown in figure 1 is commonly used in MREIT experiments. We assume that the main magnetic field is parallel to the z-direction. A current injected into the imaged object produces a magnetic flux density $\mathbf{B}$ of which only the z-component B_z is measured. We obtain the following complex k-space data $\mathcal{S}^{\pm}$ after injection of positive and negative currents, I^+ and I^-, respectively, as shown in figure 1:

$$\mathcal{S}^{\pm}(m,n) = \int\int_{-\infty}^{\infty} M(x,y)\, \mathrm{e}^{\mathrm{j}\delta(x,y)}\, \mathrm{e}^{\pm \mathrm{j}\gamma B_z(x,y)T_c}\, \mathrm{e}^{\mathrm{j}(xm\Delta k_x + yn\Delta k_y)}\, \mathrm{d}x\, \mathrm{d}y, \qquad (1)$$

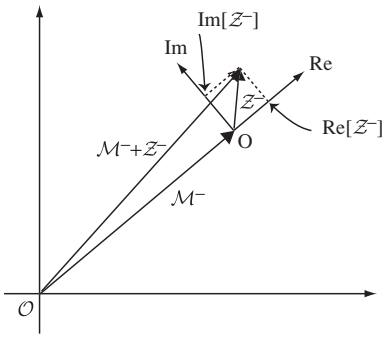

Figure 2. An example of $\mathcal{M}^-$ and $\mathcal{Z}^-$. Note the definition of the local axis for $\mathcal{Z}^-$.

where δ is any systematic phase artefact, $\gamma = 26.75 \times 10^7$ rad T^{-1} s^{-1} is the gyromagnetic ratio of hydrogen and T_c is the current pulse width in seconds. Taking two-dimensional discrete Fourier transformations, we obtain the following complex signals:

$$\mathcal{M}^{\pm}(x, y) = M(x, y)\, \mathrm{e}^{\mathrm{j}\delta(x,y)}\, \mathrm{e}^{\pm \mathrm{j}\gamma B_z(x,y)T_c}, \tag{2}$$

where $\pm B_z$ are the induced magnetic flux densities obtained with injection currents of I^+ or I^-, respectively. Note that $|\mathcal{M}^+| = |\mathcal{M}^-| = M$ is proportional to the size (volume) of voxels. In this paper, we do not consider other MR imaging parameters affecting M and δ (Haacke *et al* 1999, Bernstein *et al* 2004). The induced magnetic flux density B_z is embedded in the following incremental phase change in MR data:

$$\Psi(x, y) = \arg\left(\frac{\mathcal{M}^+(x, y)}{\mathcal{M}^-(x, y)}\right) = 2\gamma B_z(x, y)T_c, \tag{3}$$

where we assume that the operator arg(·) includes any necessary phase unwrapping (Ghiglia and Pritt 1998). In MREIT, it is essential to maximize this phase change to obtain larger B_z signals. Note that by using two current injections I^+ and I^-, we therefore reject any systematic phase artefact δ and double the phase change expressed in (3).

Once we obtain Ψ, we compute B_z as

$$B_z(x, y) = \frac{\Psi(x, y)}{2\gamma T_c} = \frac{1}{2\gamma T_c} \arg\left(\frac{\mathcal{M}^+(x, y)}{\mathcal{M}^-(x, y)}\right). \tag{4}$$

The measured $\mathcal{M}^{\pm}$ contain independent and identically distributed complex Gaussian random noise $\mathcal{Z}^{\pm}$, respectively. That is, measured signals may be described by

$$\mathcal{M}^{\pm} + \mathcal{Z}^{\pm}, \qquad \text{where} \quad \mathcal{Z}^{\pm} = r^{\pm} + \mathrm{j}i^{\pm}$$

and r^+, r^-, i^+ and i^- are identically distributed Gaussian random variables with zero mean and a variance of s^2. Figure 2 shows an example of $\mathcal{M}^-$ and $\mathcal{Z}^-$. Without loss of generality, we may set the local coordinate of $\mathcal{Z}^-$ with its real axis parallel to the direction of $\mathcal{M}^-$. Then, the noise $\mathcal{Z}^-$ can be understood as a vector located at the local origin O, having a random magnitude and direction.

Scott *et al* (1992) defined the SNR, Υ, in a noisy magnitude image $|\mathcal{M}^- + \mathcal{Z}^-|$ as

$$\Upsilon = \frac{\mathrm{mean}(|\mathcal{M}^- + \mathcal{Z}^-|)}{\mathrm{sd}(\mathcal{M}^- + \mathcal{Z}^-)} = \frac{|\mathcal{M}^-|}{\mathrm{sd}(\mathcal{Z}^-)} = \frac{M}{\sqrt{2}s}, \tag{5}$$

where mean(·) and sd(·) denote the mean and standard deviation, respectively. They derived an expression for the standard deviation in measured B_z data as

$$\mathrm{sd}(B_z) = \frac{1}{2\gamma T_\mathrm{c} \Upsilon}. \tag{6}$$

However, as shown below, we found that it is more convenient to define the SNR, Υ_M, of the magnitude image as

$$\Upsilon_\mathrm{M} = \frac{\mathrm{mean}(|\mathcal{M}^- + \mathcal{Z}^-|)}{\mathrm{sd}(|\mathcal{M}^- + \mathcal{Z}^-|)} = \frac{M}{\mathrm{sd}(|\mathcal{M}^- + \mathcal{Z}^-|)} = \frac{M}{s}. \tag{7}$$

The origin of the final equality in (7) will be clear after working through the expression in (10).

In the following section, we derive an expression for the noise standard deviation in measured B_z using the magnitude image SNR definition in (7). Including noise in (4), we now have B_z signals proportional to

$$\begin{aligned}\arg\left(\frac{\mathcal{M}^+ + \mathcal{Z}^+}{\mathcal{M}^- + \mathcal{Z}^-}\right) &= \arg\left(\frac{\mathcal{M}^+\left(1 + \frac{\mathcal{Z}^+}{\mathcal{M}^+}\right)}{\mathcal{M}^-\left(1 + \frac{\mathcal{Z}^-}{\mathcal{M}^-}\right)}\right) \\ &= \arg\left(\frac{\mathcal{M}^+}{\mathcal{M}^-}\right) + \arg\left(1 + \frac{\mathcal{Z}^+}{\mathcal{M}^+}\right) - \arg\left(1 + \frac{\mathcal{Z}^-}{\mathcal{M}^-}\right).\end{aligned} \tag{8}$$

Assuming that $|\mathcal{M}^\pm| \gg |\mathcal{Z}^\pm|$, we have $\arg\left(1 + \frac{\mathcal{Z}^\pm}{\mathcal{M}^\pm}\right) \approx \mathrm{Im}\left(\frac{\mathcal{Z}^\pm}{\mathcal{M}^\pm}\right)$. This can also be understood from figure 2, since the imaginary part of $\mathcal{Z}^-$ perturbs the argument of $\mathcal{M}^-$. Now, the standard deviation of the argument in (8) is

$$\begin{aligned}\mathrm{sd}\left[\arg\left(\frac{\mathcal{M}^+ + \mathcal{Z}^+}{\mathcal{M}^- + \mathcal{Z}^-}\right)\right] &\approx \mathrm{sd}\left[\mathrm{Im}\left(\frac{\mathcal{Z}^+}{\mathcal{M}^+}\right) - \mathrm{Im}\left(\frac{\mathcal{Z}^-}{\mathcal{M}^-}\right)\right] \\ &= \sqrt{2}\,\mathrm{sd}\left[\mathrm{Im}\left(\frac{\mathcal{Z}^-}{\mathcal{M}^-}\right)\right] = \frac{\sqrt{2}}{|\mathcal{M}^-|}\,\mathrm{sd}[\mathrm{Im}(\mathcal{Z}^-)] \\ &= \frac{\sqrt{2}}{|\mathcal{M}^-|\sqrt{2}}\,\mathrm{sd}(\mathcal{Z}^-) = \frac{1}{M}\,\mathrm{sd}(\mathcal{Z}^-).\end{aligned} \tag{9}$$

We now estimate the standard deviation of the magnitude image, $|\mathcal{M}^- + \mathcal{Z}^-|$. As shown in figure 2, the real part of the complex Gaussian random noise $\mathcal{Z}^-$ mainly perturbs the magnitude of $\mathcal{M}^-$. This can be seen by setting, without loss of generality, $\mathcal{M}^- = 1$ and $\mathcal{Z}^- = a + \mathrm{j}b$ with $a, b \ll 1$. Then,

$$|\mathcal{M}^- + \mathcal{Z}^-| = \sqrt{(1+a)^2 + b^2} = \sqrt{1 + 2a + a^2 + b^2} = 1 + a + \frac{a^2 + b^2}{2} + \cdots \approx 1 + a.$$

Therefore, we have

$$\mathrm{sd}(|\mathcal{M}^- + \mathcal{Z}^-|) \approx \mathrm{sd}(\mathrm{Re}[\mathcal{Z}^-]) = \tfrac{1}{\sqrt{2}}\,\mathrm{sd}(\mathcal{Z}^-). \tag{10}$$

Finally, we obtain an expression for the standard deviation in measured magnetic flux density B_z as

$$\mathrm{sd}(B_z) = \frac{1}{2\gamma T_\mathrm{c} |\mathcal{M}^-|}\,\mathrm{sd}(\mathcal{Z}^-) = \frac{\sqrt{2}}{2\gamma T_\mathrm{c} M}\,\mathrm{sd}(|\mathcal{M}^- + \mathcal{Z}^-|). \tag{11}$$

With the definition of SNR, Υ_M, from (7), we conclude that

$$\mathrm{sd}(B_z) = \frac{1}{\sqrt{2}\gamma T_\mathrm{c} \Upsilon_\mathrm{M}}. \tag{12}$$

Note that the expression in (12) is different from Scott *et al*'s (1992) result by a factor of $\sqrt{2}$ because of the different definitions of SNR in magnitude images.

We now describe how to estimate the magnitude image SNR, Υ_{M}, in (7) from the magnitude image of $|\mathcal{M}^- + \mathcal{Z}^-|$. Ideally, in a noise-free magnitude image $|\mathcal{M}^-|$ of a homogeneous object, we should obtain one value everywhere inside the object and zero outside. However, due to factors such as main magnetic field inhomogeneity, gradient nonlinearity and non-uniform RF coil sensitivity, we observe a non-uniform intensity profile inside the object. Outside the object, we have Rayleigh distributed noise $|\mathcal{Z}^-| = \sqrt{r^{-2} + i^{-2}}$ with a standard deviation of about $0.655s$, where s is the standard deviation of identically distributed zero-mean Gaussian random variables r^- and i^- (Haacke *et al* 1999).

To evaluate Υ_{M}, we select a region inside the object that appears the most uniform and compute the average value of all pixels within it. We select a region outside the object and compute the standard deviation of all pixels there. Then, Υ_{M} is evaluated as the average value times 0.655 divided by the standard deviation. Alternatively, we may compute both the average value and standard deviation in the region chosen inside the object. Then, Υ_{M} is simply the ratio of the average value over the standard deviation.

2.2. Noise estimation method 2

In this section, we proceed from the measured magnetic flux density B_z in (4). We express the noise-contaminated measured magnetic flux density $\tilde{B}_z$ as

$$\tilde{B}_z = B_z + \eta, \tag{13}$$

where η is a Gaussian random variable with zero mean and variance of $s^2_{B_z}$. Although the noise distribution in phase data is not in general Gaussian, particularly at low signal-to-noise ratios (Gudbjartsson and Patz 1999), we assume that the system SNR is sufficiently high to allow this approximation. Note that the standard deviation s_{B_z} must be equal to $\mathrm{sd}(B_z)$ in (12). Here, values of even noise-free B_z data are not uniform and depend on the geometry and conductivity of the imaging object as well as the electrode configuration and injection current magnitude (Lee *et al* 2003b). Therefore, we seek a way to eliminate B_z from $\tilde{B}_z$ so as to extract only the noise η in order to evaluate its standard deviation alone.

As shown by Seo *et al* (2003) and Oh *et al* (2003), when the conductivity distribution σ of the imaging object is homogeneous, for example, $\sigma = 1$, we have

$$\nabla^2 B_z = 0. \tag{14}$$

Applying this to (13), we obtain

$$\nabla^2 \tilde{B}_z = \nabla^2 \eta. \tag{15}$$

We assume that the image of $\tilde{B}_z$ is obtained as a three-dimensional matrix $\tilde{B}_z(l, m, n)$ with $l, m, n = 1, \ldots, N$. Therefore, the second-order differentiation in (15) may be expressed as

$$\begin{aligned}\nabla^2 \tilde{B}_z(l,m,n) = {} & \frac{1}{\Delta^2}[\eta(l+1,m,n) + \eta(l-1,m,n) + \eta(l,m+1,n) + \eta(l,m-1,n)] \\ & - \frac{4}{\Delta^2}\eta(l,m,n) + \frac{1}{\Delta_z^2}[\eta(l,m,n+1) + \eta(l,m,n-1)] - \frac{2}{\Delta_z^2}\eta(l,m,n),\end{aligned} \tag{16}$$

where $\Delta = \Delta_x = \Delta_y$ is the distance between consecutive pixels along the x- and y-directions, and Δ_z is the slice thickness. Since all η are identically distributed Gaussian random variables

Table 1. Noise parameters measured in 3 and 11 T MREIT experiments. NEX is the number of excitations or averages. The voxel size is $1 \times 1 \times 1$ mm^3.

Field strength in T	3		11	
NEX	1	4	1	4
Υ_M in (7)	11.8	22.2	59.6	123
sd(B_z) of (12) in nT	13.9	7.54	2.73	1.32
s_{B_z} of (18) in nT	15.0	6.72	2.91	1.35

with zero mean and variance of $s^2_{B_z}$, the variance of $\nabla^2 \tilde{B}_z(l, m, n)$ can be expressed as

$$\begin{aligned} s^2_{\nabla^2 \tilde{B}_z} &= \left(\frac{1}{\Delta^2} s_{B_z}\right)^2 \times 4 + \left(\frac{4}{\Delta^2} s_{B_z}\right)^2 + \left(\frac{1}{\Delta_z^2} s_{B_z}\right)^2 \times 2 + \left(\frac{2}{\Delta_z^2} s_{B_z}\right)^2 \\ &= \left(\frac{20}{\Delta^4} + \frac{6}{\Delta_z^4}\right) s^2_{B_z}, \end{aligned} \tag{17}$$

where $s_{\nabla^2 \tilde{B}_z}$ is the standard deviation of the Gaussian random noise in $\nabla^2 \tilde{B}_z$.

This means that the second-order differentiation of $\nabla^2 \tilde{B}_z$ increases the noise power by a ratio of $\frac{26}{\Delta^4}$ if $\Delta_z = \Delta$. Since we can directly estimate $s^2_{\nabla^2 \tilde{B}_z}$ from calculated $\nabla^2 \tilde{B}_z$ values, the relation of (17) provides a way to experimentally estimate standard deviation s_{B_z} in measured $\tilde{B}_z$ data by

$$s_{B_z} = \frac{1}{\sqrt{\frac{20}{\Delta^4} + \frac{6}{\Delta_z^4}}} s_{\nabla^2 \tilde{B}_z}. \tag{18}$$

Gathering $\tilde{B}_z$ data using a homogeneous conductivity phantom, we may also evaluate the relation in (18). If s_{B_z} in (18) and sd(B_z) in (12) are approximately equal to each other, we can confirm that the MREIT experiment is consistent. Otherwise, we conclude that the experiment contained systematic artefacts in measured $\tilde{B}_z$ data in addition to Gaussian random noise.

2.3. MREIT experiments

We constructed an acrylic phantom filled with a solution (1 g l^{-1} $CuSO_4$ and 3.125 g l^{-1} NaCl) whose conductivity was 0.625 S m^{-1}. On the middle of each side, a recessed electrode assembly was attached to inject currents into the phantom.

To measure the corresponding internal magnetic flux density B_z, we used the pulse sequence shown in figure 1. The injection current magnitude was $I = 10$ mA and the total current pulse width was $T_c = 16$ ms. We performed the experiment using both the 3 T MRI scanner (Medinus, Korea) at the Impedance Imaging Research Center (IIRC), Kyung Hee University, Korea and the 11 T MRI scanner (Bruker Biospin, Germany) at the McKnight Brain Institute, University of Florida, USA. In order to make the noise levels comparable, we used the same voxel size of $1 \times 1 \times 1$ mm^3 and similar MR imaging parameters.

3. Results

Noise statistic estimations are summarized in table 1. As expected, when the number of averages (NEX) was 4, the magnitude image SNR, Υ_M, was increased by a factor of about 2 and the noise level in B_z was reduced by the same factor. On increasing the main magnetic field strength from 3 to 11 T, we found a reduction in the noise level by a factor of about 5.

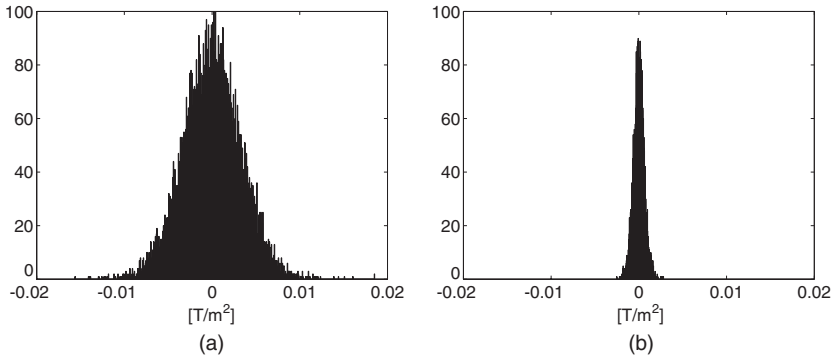

Figure 3. Histograms of $\nabla^2 \tilde{B}_z$ at (a) 3 T and (b) 11 T.

Figures 3(a) and (b) show histograms of $\nabla^2 \tilde{B}_z$ for 3 and 11 T data, respectively. The much narrower histogram in (b) demonstrates the smaller noise standard deviation in measured B_z data from the 11 T experiment.

The noise estimates found independently using (12) and (18) were in a good agreement, suggesting that there were few systematic artefacts in the experiments. We propose that these two methods of estimating the noise level in measured B_z data can be used to validate and verify an MREIT experimental setup.

4. Discussion

In MREIT, the raw data measured is the incremental phase change, as shown in (3). This phase change is proportional to the product of B_z and T_c. Therefore, we must optimize the MREIT pulse sequence to maximize the product of I and T_c in figure 1, since B_z is directly proportional to I. When imaging *in vivo*, maximizing $I \cdot T_c$ must naturally be performed subject to electrical safety requirements (Reilly 1998).

Noise levels in 11 T data were found in this investigation to be five times smaller than those found in 3 T data. However, since the MR imaging parameters were not exactly identical in the 3 and 11 T data used in this paper, we do not argue that the ratio holds between any 3 and 11 T MREIT experiments. This ratio should be understood as a rough estimate of the advantage gained by using 11 T instead of 3 T. We plan to perform further experiments to make a better estimate of this factor. In particular, we will carefully consider the impact of factors such as TR/TE, slice profile and the RF coil fill factor on noise, since all of these also affect SNR.

The two methods of estimating the noise level in measured $\tilde{B}_z$ data provide a way to validate settings in an MREIT experiment. When the noise level computed by (18) is greater than the value by (12), we can suppose that the experimental settings produced a significant amount of systematic phase artefact. In this case, we may estimate the amount of artefact by setting

$$\tilde{B}_z = B_z + \eta + \xi,$$

where ξ is the artefact. Mathematically, we have

$$B_z(\mathbf{r}) + \eta(\mathbf{r}) + \xi(\mathbf{r}) = \int_\Omega \frac{1}{4\pi |\mathbf{r} - \mathbf{r}'|} \nabla^2 \tilde{B}_z(\mathbf{r}')\, \mathrm{d}\mathbf{r}' + h(\mathbf{r}),$$

where $\mathbf{r}, \mathbf{r}'$ are position vectors and h is a harmonic function inside the object of interest Ω, which depends on the Dirichlet and Neumann boundary conditions applied to $\tilde{B}_z$ on the object boundary $\partial\Omega$. Since η and ξ are usually independent of these boundary conditions, we propose the following approximation:

$$\eta(\mathbf{r}) + \xi(\mathbf{r}) \approx \int_\Omega \frac{1}{4\pi|\mathbf{r}-\mathbf{r}'|}\nabla^2\tilde{B}_z(\mathbf{r}')\,\mathrm{d}\mathbf{r}',$$

for $\mathbf{r}$ inside Ω. Using Gaussian blurring to eliminate the noise η, we can compute the artefact roughly as

$$\xi(\mathbf{r}) \approx \int_\Omega \frac{1}{4\pi|\mathbf{r}-\mathbf{r}'|}\nabla^2 G(\tilde{B}_z)\,\mathrm{d}\mathbf{r}',$$

where G is a Gaussian blurring operation.

The most basic factor determining the quality of reconstructed conductivity and current density images in MREIT is the SNR in measured B_z data. However, in this paper, we have not analysed B_z data directly. As described in Lee *et al* (2003b), the distribution of B_z is not spatially uniform, making it difficult to define signal strength and therefore immediately estimate the SNR in B_z (although analysis of B_z noise in images gathered without current injection will serve to provide a lower bound for the noise level). Therefore, we must choose a signal parameter with a direct relation to conductivity and compare it to the amount of the noise in measured B_z data. Since $\mathbf{J} = \nabla \times \mathbf{B}/\mu_0 = -\sigma\nabla u$, where $\mathbf{J}$ is the current density, $\mathbf{B}$ is magnetic flux density and u is the voltage, the quantity $|\nabla B_z|/|\nabla u|$ is closely related to the conductivity σ. This suggests that a comparison between $|\nabla B_z|$ and the noise gradient $\mathrm{sd}(|\nabla\eta|)$ (as in (13)) might be made. However, the way we process the measured three-dimensional B_z maps during conductivity image reconstructions also significantly affects image quality. Therefore, we are currently trying to determine the relationships between MR parameters, noise values and electrode configurations in order to establish their effect on image quality. In addition, we are investigating the sensitivity of B_z or any chosen signal parameter to a local change of the conductivity.

From the results in table 1, it appears possible to obtain B_z data with standard deviations of less than 0.25 or 0.05 nT from 3 or 11 T MREIT systems, respectively, by increasing the voxel size to $3 \times 3 \times 3$ mm^3. Increasing the number of averages and/or T_c could be tried to further reduce noise levels. At a field strength of 3 T, we speculate that a noise level below 0.1 nT could readily be achieved. With this intrinsic level of noise, MREIT imaging using injection currents less than 5 mA may be possible. A more thorough study of image quality and sensitivity in MREIT will be a part of our future studies to provide much concrete experimental design criteria.

5. Conclusion

We rigorously derived an expression for the standard deviation of measured magnetic flux density data in MREIT. We also suggested an alternative method to estimate noise levels when using an imaging object with a homogeneous conductivity distribution. Using MREIT systems at 3 and 11 T main magnetic field strengths, we found that the noise level in measured magnetic flux density is reduced as field strength is increased, and that the reduction factor seems to be approximately proportional to the increase in the field strength. The two methods of analysing noise levels are useful to validate an MREIT experimental setup.

Using a voxel size of $3 \times 3 \times 3$ mm^3, we found that noise levels in B_z could be reduced to about 0.25 or 0.05 nT at 3 or 11 T field strength, respectively. In order to further reduce noise levels, a more detailed investigation to optimize MREIT pulse sequences must be undertaken.

At the same time, experimental and data processing techniques to reduce noise must be considered.

Acknowledgments

This work was supported by the Advanced Magnetic Resonance Imaging and Spectroscopy (AMRIS) facility at the McKnight Brain Institute, University of Florida, USA and grants R11-2002-103/M60501000035-05A0100-03510 from the Korea Science and Engineering Foundation (KOSEF), Korea.

References

Bernstein M A, King K F and Zhou X J 2004 *Handbook of MRI Pulse Sequences* (Burlington, MA: Elsevier)

Birgul O, Eyuboglu B M and Ider Y Z 2003 Current constrained voltage scaled reconstruction (CCVSR) algorithm for MR-EIT and its performance with different probing current patterns *Phys. Med. Biol.* **48** 653–71

Ghiglia D C and Pritt M D 1998 *Two-Dimensional Phase Unwrapping: Theory, Algorithms and Software* (New York, NY: Wiley-Interscience)

Gudbjartsson H and Patz S 1995 The Rician distribution of noisy MRI data *Magn. Reson. Med.* **34** 910–4

Haacke E M, Brown R W, Thompson M R and Venkatesan R 1999 *Magnetic Resonance Imaging: Physical Principles and Sequence Design* (New York, NY: Wiley)

Ider Y Z and Birgul O 1998 Use of the magnetic field generated by the internal distribution of injected currents for electrical impedance tomography (MR-EIT) *Elektrik* **6** 215–25

Ider Y Z and Onart S 2004 Algebraic reconstruction for 3D MR-EIT using one component of magnetic flux density *Physiol. Meas.* **25** 281–94

Ider Y Z, Onart S and Lionheart W R B 2003 Uniqueness and reconstruction in magnetic resonance-electrical impedance tomography (MR-EIT) *Physiol. Meas.* **24** 591–604

Khang H S, Lee B I, Oh S H, Woo E J, Lee S Y, Cho M H, Kwon O, Yoon J R and Seo J K 2002 J-substitution algorithm in magnetic resonance electrical impedance tomography (MREIT): phantom experiments for static resistivity images *IEEE Trans. Med. Imaging* **21** 695–702

Kim T S, Lee B I, Lee S H, Seo J K, Kwon O and Woo E J 2004 Diffusion PDE-based denoising technique for magnetic resonance electrical impedance tomography *Proc. 26th Annu. Int. Conf. IEEE EMBS (San Francisco, CA)* pp 1036–9

Kwon O, Park C, Park E J, Seo J K and Woo E J 2005 Electrical conductivity imaging using a variational method in B_z-based MREIT *Inverse Problems* **21** 969–80

Kwon O, Woo E J, Yoon J R and Seo J K 2002 Magnetic resonance electrical impedance tomography (MREIT): simulation study of J-substitution algorithm *IEEE Trans. Biomed. Eng.* **48** 160–7

Lee B I, Oh S H, Woo E J, Lee S Y, Cho M H, Kwon O, Seo J K and Baek W S 2003a Static resistivity image of a cubic saline phantom in magnetic resonance electrical impedance tomography (MREIT) *Physiol. Meas.* **24** 579–89

Lee B I, Oh S H, Woo E J, Lee S Y, Cho M H, Kwon O, Seo J K, Lee J Y and Baek W S 2003b Three-dimensional forward solver and its performance analysis in magnetic resonance electrical impedance tomography (MREIT) using recessed electrodes *Phys. Med. Biol.* **48** 1971–86

Oh S H, Lee B I, Park T S, Lee S Y, Woo E J, Cho M H, Kwon O and Seo J K 2004 Magnetic resonance electrical impedance tomography at 3 tesla field strength *Magn. Reson. Med.* **51** 1292–6

Oh S H, Lee B I, Woo E J, Lee S Y, Cho M H, Kwon O and Seo J K 2003 Conductivity and current density image reconstruction using harmonic B_z algorithm in magnetic resonance electrical impedance tomography *Phys. Med. Biol.* **48** 3101–16

Oh S H, Lee B I, Woo E J, Lee S Y, Kim T S, Kwon O and Seo J K 2005 Electrical conductivity images of biological tissue phantoms in MREIT *Physiol. Meas.* **26** S279–88

Park C, Kwon O, Woo E J and Seo J K 2004a Electrical conductivity imaging using gradient B_z decomposition algorithm in magnetic resonance electrical impedance tomography (MREIT) *IEEE Trans. Med. Imaging* **23** 388–94

Park C, Park E J, Woo E J, Kwon O and Seo J K 2004b Static conductivity imaging using variational gradient B_z algorithm in magnetic resonance electrical impedance tomography *Physiol. Meas.* **25** 275–69

Reilly J P 1998 *Applied Bioelectricity: From Electrical Stimulation to Electropathology* (New York, NY: Springer)

Scott G C, Joy M L G, Armstrong R L and Henkelman R M 1991 Measurement of nonuniform current density by magnetic resonance *IEEE Trans. Med. Imaging* **10** 362–74

Scott G C, Joy M L G, Armstrong R L and Henkelman R M 1992 Sensitivity of magnetic resonance current density imaging *J. Magn. Reson.* **97** 235–54

Seo J K, Yoon J R, Woo E J and Kwon O 2003 Reconstruction of conductivity and current density images using only one component of magnetic field measurements *IEEE Trans. Biomed. Eng.* **50** 1121–4

Woo E J, Lee S Y and Mun C W 1994 Impedance tomography using internal current density distribution measured by nuclear magnetic resonance *Proc. SPIE* **2299** 377–85

Zhang N 1992 Electrical impedance tomography based on current density imaging *MS Thesis* Department of Electrical Engineering, University of Toronto, Toronto, Canada